

**Key Points:**

- Tropical cyclone (TC) activity is reduced in multiple global climate models using a novel algorithm to suppress evaporation
- TC frequency is reduced by approximately 50% for all intensities, with hurricane-strength TC frequency reduced by over 90%
- TC with suppressed evaporation feature lower peak intensities and shorter spatial ranges than unmodified TCs

Correspondence to:

G. Rios,
gr7610@princeton.edu

Citation:

Rios, G., Vecchi, G., & Yang, W. (2025). Reducing tropical cyclone activity in global climate models by evaporative suppression. *Journal of Geophysical Research: Atmospheres*, 130, e2024JD043302. <https://doi.org/10.1029/2024JD043302>

Received 13 JAN 2025

Accepted 3 JUL 2025

Author Contributions:

Conceptualization: Gabriel Rios, Gabriel Vecchi, Wenchang Yang
Formal analysis: Gabriel Rios
Funding acquisition: Gabriel Rios, Gabriel Vecchi
Investigation: Gabriel Rios, Gabriel Vecchi, Wenchang Yang
Methodology: Gabriel Rios, Gabriel Vecchi, Wenchang Yang
Project administration: Gabriel Vecchi, Wenchang Yang
Resources: Gabriel Vecchi, Wenchang Yang
Software: Gabriel Rios, Gabriel Vecchi, Wenchang Yang
Supervision: Gabriel Vecchi, Wenchang Yang
Validation: Gabriel Vecchi, Wenchang Yang
Visualization: Gabriel Rios
Writing – original draft: Gabriel Rios

© 2025 The Author(s).

This is an open access article under the terms of the Creative Commons Attribution-NonCommercial License, which permits use, distribution and reproduction in any medium, provided the original work is properly cited and is not used for commercial purposes.

Reducing Tropical Cyclone Activity in Global Climate Models by Evaporative Suppression

Gabriel Rios^{1,2} , Gabriel Vecchi^{2,3} , and Wenchang Yang² 

¹Program in Atmospheric and Oceanic Sciences, Princeton University, Princeton, NJ, USA, ²Department of Geosciences, Princeton University, Princeton, NJ, USA, ³High Meadows Environmental Institute, Princeton, NJ, USA

Abstract What would a world without tropical cyclones look like? Although such a world is unrealistic, addressing this question would reveal the role tropical cyclones (TCs) play in modulating the climate system. In this study, we begin to address this question by introducing a novel algorithm for reducing TC activity in TC-permitting global climate models (GCMs) through suppression of wind-induced surface heat exchange (WISHE) at grid points where TC-like conditions are detected. This algorithm, abbreviated as “SWISHE,” was implemented in a suite of GCM simulations developed by NOAA’s Geophysical Fluid Dynamics Laboratory and compared to a control suite of simulations with no perturbations. Application of SWISHE resulted in a model-mean 44% reduction of TC frequency compared to control simulations, with TCs of hurricane-strength reduced by approximately 90%. Aggregate analysis of TCs reveals that TCs in the SWISHE simulations are weaker, as peak 10-m horizontal wind speeds decrease by a model-mean of 3.9 m s^{-1} and minimum sea-level pressures increase by a model-mean of 4.7 hPa. Composite analysis is used to confirm that SWISHE effectively suppressed latent heat fluxes in grid cells with TC-like conditions. The results presented herein are intended to provide a first step in establishing methodology to understand upscale impacts of TCs on the climate system.

Plain Language Summary Tropical cyclones (also known as hurricanes or typhoons, abbreviated as TCs) are among the most powerful naturally occurring phenomena and pose significant risks to life and property. As the climate changes, TC activity and intensity are also expected to change due to shifts in large-scale factors such as ocean temperatures and atmospheric moisture. Given that TCs are such powerful phenomena, it is expected that changes to TC activity and intensity will also impact the climate. However, the impacts of TCs on the climate are not yet well-understood. This study uses a novel algorithm to improve understanding of TC impacts on climate by using global climate models (GCMs) to produce a climate with fewer and weaker TCs. This algorithm, abbreviated as SWISHE, suppresses evaporation in portions of the GCM domain with TC-like conditions. Across all GCMs used, application of SWISHE resulted in a climate with 44% fewer TCs compared to a control climate, with the subset of TCs reaching hurricane intensity being reduced by 90%. These results show the effectiveness of SWISHE in reducing TC activity and suggest that this algorithm can serve as a starting point for understanding effects of TCs on the climate system.

1. Background

The effects of the climate on tropical cyclones have been the subject of considerable scientific attention and are becoming well-understood (Camargo & Sobel, 2005; Donnelly & Woodruff, 2007; K. Emanuel et al., 2004). Decades of attention have helped uncover the effects of climatic factors on tropical cyclone (TC) formation and intensification; for example, it is known that factors such as warm sea-surface temperatures (SST), a moist mid-tropospheric layer, a cool upper troposphere, high cyclonic vorticity, large-scale ascent, and low vertical wind shear foster a hospitable environment for TCs (Corbosiero & Molinari, 2002; K. A. Emanuel, 1986; Hsieh et al., 2020; Tang & Emanuel, 2010). The effects of climate change on TCs have also been widely investigated. Although a definitive consensus on how climate change impacts TCs has not been reached, there is a growing consensus that global warming and changes to anthropogenic emissions will increase TC intensity and rainfall associated with TCs (Knutson et al., 2010; Reed et al., 2022; Scoccimarro et al., 2014; Walsh et al., 2016). However, the upscale effects of TCs on climate (small-scale on large-scale) have been studied far less. TCs have been hypothesized to influence climate for decades (Fisher, 1958; Gangopadhyaya & Riehl, 1959). To the authors’ knowledge, most studies of the effects of TCs on climate have focused on oceanic impacts, whereas studies exploring the atmospheric effects of TCs on climate are more limited (K. Emanuel, 2008; Scoccimarro et al., 2020).

Writing – review & editing: Gabriel Rios,
Gabriel Vecchi, Wenchang Yang

The effects of TCs on the ocean have been studied for decades. A consistent finding from the earliest studies of TC feedbacks onto the ocean are their impact on sea surface cooling due to upper ocean mixing using observational and numerical methods. This was noted in early observations of the ocean surface after the passage of several TCs in the North Atlantic and Gulf of Mexico, respectively. Additional work using several observational techniques (Hazelworth, 1968; Holt, 1976; Leipper, 1967; Lloyd & Vecchi, 2011; Sanford et al., 1987; Stramma et al., 1986) found similar trends of upper ocean cooling and mixing after TC passage. Numerical studies of this phenomenon demonstrated that upwelling, entrainment, and horizontal divergence of heat fluxes are primary contributors to cooling in the thermocline (Jacob et al., 2000; O'Brien & Reid, 1967; Price, 1981). Given the effects of TCs on heat content in the upper ocean, their influence on ocean heat transport has been studied. K. Emanuel (2001) estimated ocean heating by TCs during a given year on the order of 10^{15} W due to the aforementioned processes, which is significant relative to the amount of poleward heat flux transported by the oceans. Srivastava and Huber (2007) used observational data and Scoccimarro et al. (2011) used a high-resolution global climate model to provide evidence supporting this phenomenon, as well as finding that TCs increase poleward heat fluxes. These findings are significant to elucidating the role of TCs on climate, as the increase in poleward fluxes serves to regulate tropical climate and increase climatic sensitivity at higher latitudes. Several other studies have also emphasized the role of TCs on ocean thermodynamics and consequential effects on the climate (K. Emanuel, 2008; Gutiérrez Brizuela et al., 2023; Manucharyan et al., 2011; Srivastava & Huber, 2010; Sobel & Camargo, 2005; Sun et al., 2021).

The effects of TCs on the atmosphere are less understood, although several studies have made progress toward understanding them using observational techniques. Sobel and Camargo (2005) presented, to the authors' knowledge, one of the first analyses attempting to understand the role of TCs on the atmosphere by using a lag regression on composite observations of environmental variables related to TC activity (using the accumulated cyclone energy, or ACE, metric), which provided a novel framework for examining TC influences. The study found increases in outgoing longwave radiation and column-integrated water vapor, as well as reductions in sea-surface temperatures (SSTs) and 500 hPa temperature. Hart et al. (2007) and Schenkel and Hart (2015) built upon the observational lead-lag framework by exploring potential TC signatures on the atmosphere at different intervals after passing, finding evidence of its effects by revealing Rossby wave packets associated with TCs, long-term negative moist static energy anomalies, and also finding increasing outgoing longwave radiation signals as a potential effect of drying caused by TCs passing through the domains evaluated. The use of high-ACE and low-ACE years as a method to observationally reveal the effects of TCs on the atmosphere for a given basin was performed by Scoccimarro et al. (2020) in conjunction with climate model simulations, finding that TC activity in the western North Pacific TCs positively correlates with reduced precipitation over the Maritime Continent, suggesting the potential for TCs to impact large-scale circulation patterns and moisture transport. The hydrological and radiative impacts of TCs have been increasingly explored in the literature with the increased availability of high-resolution observational and climate model data (Hu et al., 2023; Pérez-Alarcón et al., 2023).

Despite the contributions afforded by these observational studies, these analyses are performed with TCs still present in the climate system and their impacts modulate climate in ways that are not well-understood. Ideally, a clean approach to understand how TCs influence climate would involve removing all TCs from the system and comparing such a climate to a typical climate state; in other words, a mechanism denial experiment, where the mechanism is the TC. Several attempts have been made to accomplish this using numerical studies, albeit in highly idealized domains that are spatially limited (Ma & Fei, 2022; Murthy & Boos, 2018; Wang & Lin, 2020; F. Zhang & Emanuel, 2016). Several studies examining the suppression of TCs begin to remove idealizations by using atmospheric models with multiple vortices in periodic domains such that inter-phenomena effects are represented (Cronin & Chavas, 2019; Muller & Romps, 2018; Reyes & Yang, 2021). Further adding a degree of realism, a few studies have used realistic WRF setups in different configurations to observe the effects of TC suppression (Bercos-Hickey & Patricola, 2023; Danso et al., 2022; Patricola et al., 2016; Peng & Wu, 2020; Shen et al., 2021). However, these numerical studies have focused on the effects of TC suppression on storm properties, rather than the effects of TC suppression outside their domains.

To address this gap in knowledge, we introduce a new method to suppress TC activity in a global climate model (GCM) such that the climatic effects of TCs can be analyzed. The goal of this method is to strengthen the understanding of multiscale TC impacts in TC-permitting climate models to help address the motivating question:

how do TCs influence the large-scale climate? The algorithm used to suppress TC activity is named “SWISHE” (suppressed wind-induced surface heat exchange), which is derived from the “WISHE” acronym coined in Yano and Emanuel (1991). This method is implemented by suppressing the winds used to determine the evaporation rate, alluding to the feedback mechanism introduced in K. A. Emanuel (1986) and Rotunno and Emanuel (1987). WISHE was chosen as the mechanism to target for TC suppression for theoretical and implementation reasons. The theoretical reasoning stems from WISHE being one of the critical mechanisms for TC intensification after genesis; if WISHE is suppressed, several studies indicate that TC intensification will be limited (Craig & Gray, 1996; F. Zhang & Emanuel, 2016). The implementation choice stems from WISHE being straightforward to target in a GCM, given that the algorithm can be applied on individual grid cells (see Section 2 for details on implementation). It is worth noting that this method addresses TC intensification rather than TC genesis, which is controlled by other mechanisms, such as conditional instability of the second kind (CISK) (Craig & Gray, 1996) and radiative interactions (B. Zhang et al., 2021), rather than WISHE. By suppressing the WISHE feedback mechanism, we anticipate TCs to form, although we expect their development to be arrested due to a reduction in ocean-to-atmosphere enthalpy fluxes. The present manuscript focuses on documenting the SWISHE methodology and its impact on TCs in GCMs, with subsequent work intended to focus on the upscale influence of TC removal from GCM simulations.

This paper details the methods used and the results obtained using the SWISHE algorithm. Section 2 discusses the methodology and GCM configurations used in this study. Section 3 compares results from GCM runs in a control configuration and in a configuration using the SWISHE algorithm. The results include an evaluation of the effectiveness of SWISHE on aggregate TC activity by comparing TC frequency and intensity statistics in the control and SWISHE configurations of each model run, as well as the effect of SWISHE on TC properties at the storm scale using compositing analysis. Section 4 summarizes the results presented in Section 3, discusses the utility of the algorithm for analyzing the effects of TC activity on the climate system, and presents potential improvements for the SWISHE algorithm to address methodological shortcomings.

2. Methods and Model Configuration

2.1. SWISHE Algorithm

SWISHE is conditionally implemented in the atmosphere-ocean coupler module of the GFDL GCMs used herein on each model grid cell. SWISHE is computed at each model timestep such that latent heat fluxes (LHF) are suppressed during the model integration. The condition of implementation is determined by model parameters at each grid cell at the surface and throughout the atmospheric column corresponding to the given grid cell, as expressed in Equation 1. These parameters are chosen to represent environmental properties characteristic of the inner cores of TCs. The parameters and their corresponding values are (a) 10 m horizontal wind speeds (V) exceeding 15 m s^{-1} , (b) SST exceeding 25°C , (c) absolute values of relative vorticity (ζ_{850}) exceeding $1 \times 10^{-4} \text{ s}^{-1}$, (d) and relative humidity (RH) values exceeding 60%, 70%, and 75% at 500, 700, and 850 hPa, respectively. At grid points where parameters (a) and (b) are satisfied, a weighted index using parameters (c) and (d) is calculated to target grid points with atmospheric conditions characteristics of TCs.

The equation used to calculate this index is expressed in Equation 1.

$$n = 0.5(\text{RH}_{500} \geq 60) + (\text{RH}_{700} \geq 70) + (\text{RH}_{850} \geq 75) + 0.5(|\zeta_{850}| \geq 1 \times 10^{-4}) \quad (1)$$

Each term in Equation 1 represents a boolean expression, where the parenthetical term equals 1 if the condition is true and 0 if false. The index n in Equation 1 is constructed such that each boolean parameter is given a certain weight, and the weighted sum of these parameters must exceed a predetermined threshold. As an example, consider the first term on the right-hand side of Equation 1 corresponding to RH_{500} ; if RH_{500} is greater than or equal to 60% for a given grid cell, then the parenthetical term equals 1 and is multiplied by the 0.5 factor. Therefore, the potential values of the right-hand side of Equation 1 range from 0 to 3. The predetermined threshold ($n = 2.5$) must be met or exceeded to induce the suppression of wind speeds used for calculating LHF (V_{LHF}) when V exceeds the absolute threshold of 15 m s^{-1} .

In the GCMs used, surface fluxes are calculated as a function of a bulk transfer coefficient, 10 m horizontal wind speeds, and the vertical gradient of near-surface quantities: temperature for sensible heat flux (SHF) and specific

Table 1*List of Global Climate Models and Experiments Performed for Evaluating the SWISHE Algorithm*

Model	Configuration	Components	Ocean boundary condition
HiRAM	Control	Atmosphere only	HadISSTv1.1 monthly
	SWISHE		SST climatology (1986–2005)
AM2.5	Control	Atmosphere only	HadISSTv1.1 monthly
	SWISHE		SST climatology (1986–2005)
FLOR	Control	Coupled atmosphere-ocean	Interactive ocean model (Vecchi et al., 2014)
	SWISHE		

humidity for LHF. The suppression of wind speeds refers to a reduction of V_{LHF} as a function of Equation 1, where V_{LHF} is reduced to 0 such that LHF is also reduced to 0 when $n \geq 2.5$. The suppression of wind speeds is implemented by multiplying V_{LHF} by a factor c , where $c = 0$ if the condition in Equation 1 is true and 0 if the condition is false. This algorithm does not modify wind speeds in the atmospheric model nor wind stresses passed through the atmosphere-ocean coupler in the coupled model used (see Section 2.2 for a description of the models used). The weights, as well as the threshold, were chosen by tuning their values to match TC frequencies in each basin, such that the frequency of SWISHE application would match the TC climatology. The intended result is that the SWISHE algorithm only targets grid cells experiencing TC conditions while avoiding the suppression of evaporation for atmospheric phenomena featuring properties similar to TCs. This value was obtained through preliminary tests of the algorithm with lower n values, which resulted in partial suppression of weaker or larger-scale mesoscale convective systems (e.g., South Asian monsoon, strong mesoscale convective systems, etc.).

We note that implementing a method that is applied on a domain-like basis rather than on an individual grid cell basis (e.g., a box spanning the size of a TC, a circle encompassing the TC and its immediate surroundings, etc.) may result in more effective suppression of evaporation, but leave this for future investigation due to the risk of increased computational complexity and expense. Additional discussion regarding potential shortcomings and improvements to the methodology is provided in Section 4.

2.2. Global Climate Models

To evaluate the effectiveness of the SWISHE method, a suite of GCM simulations used in control (unmodified) and experiment (modified using SWISHE) configurations were performed. The simulations performed are described in Table 1. The suite of GCMs consists of two atmosphere-only models, AM2.5 and HiRAM, and a coupled atmosphere-ocean model, FLOR. FLOR (Forecast Low-Ocean Resolution, Vecchi et al. (2014)) is a modification of the GFDL coupled model, CM2.5 (Delworth et al., 2012), that reduces ocean and sea ice resolution to increase computational efficiency. The decreased ocean and ice resolutions are adequate for the purpose of this study, which is focused on atmospheric phenomena (i.e., TCs). AM2.5 (Atmospheric Model, version 2.5) is the atmospheric component of CM2.5 and FLOR, which is run with fixed SST prescribed as a repeated monthly climatology computed from the United Kingdom's Met Office Hadley Centre Sea Ice and Sea Surface Temperature data set (Rayner et al., 2003) averaged from years 1986–2005. HiRAM (High-Resolution Atmospheric Model, Zhao et al. (2009)) is an atmosphere-only model that uses AM2.1 (an earlier version of the atmospheric component of CM2.5) as a baseline configuration but increases the number of vertical levels and replaces a relaxed Arakawa-Schubert convective closure with a parameterization of shallow convection (Bretherton et al., 2004). However, HiRAM is modified from this scheme to improve the representation of deep convection in the GCM by modifying the convective parameterization to match the observed TC climatology (Zhao et al., 2009, 2012).

The atmospheric component of all GCMs features a horizontal resolution of approximately 0.5° with 32 vertical levels. Although the GCMs are unable to resolve small-scale TC processes, and by extension, the intensity distribution of observed TCs at this spatial resolution, studies have shown that the models used effectively reproduce the spatial distributions and frequencies of observed TCs (Kim et al., 2018; Vecchi et al., 2014; Wing et al., 2019; Zhao et al., 2009). The GCMs use a 3 hr timestep for atmospheric radiation and a 0.5 hr timestep for atmospheric physics (Delworth et al., 2006). The atmosphere-only simulations were run for 50 years after a 10 years spinup period, while FLOR was run for 200 years with the SWISHE algorithm to allow for equilibration

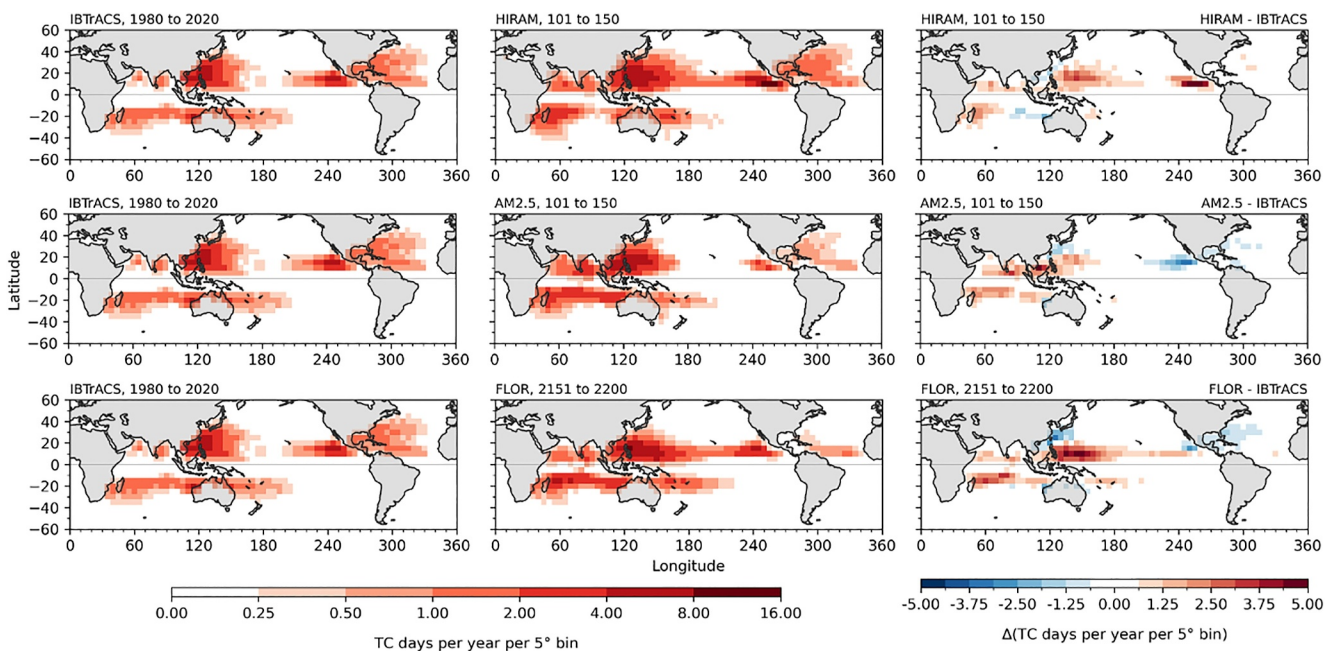


Figure 1. Density maps of Tropical cyclone (TC) locations for observed TCs obtained from observed best-track (IBTrACS) and simulated TCs from control configurations of the GCMs used in this study (HiRAM, AM2.5, FLOR). Density is calculated per model grid cell by the number of days experiencing a TC per year, grouped by $5^\circ \times 5^\circ$ spatial bins. Rows indicate different GCMs, left and center columns correspond to observed best-track and GCM TC densities, and the right column corresponds to the difference (GCM—observed best-track).

to the implementation of SWISHE, following a spinup period of 2,000 model years of the control configuration to allow for the coupled atmosphere-ocean system to reach quasi-steady state. All model integrations use a historical radiative forcing scenario with levels from the year 1990, based on the Coupled Model Intercomparison Project Phase 5 (CMIP5, (Taylor et al., 2012)). Tropical cyclone data used in this analysis samples the last 50 years of all model runs.

2.3. Comparison of Observed and Simulated TC Properties

To determine the ability of the analyzed GCMs to reproduce observed TC characteristics, we compare properties of observed TC and TCs simulated in the GCMs used in this study. Best-track data for observed TCs are obtained using the International Best Track Archive for Climate Stewardship (IBTrACS) data set (Knapp et al., 2010) over the period from 1980 to 2020. Observed TCs possessing tropical-storm strength at minimum, which is defined as 1 min-sustained 10 m wind speeds exceeding 17.5 m s^{-1} as in Murakami et al. (2016), were used for comparison with modeled TCs. Note that this section focuses on comparisons between observed and simulated TCs in the control configurations of the GCMs used in this study; intermodel differences in spatial and intensity distributions are discussed in Section 3.

The GCMs used in this study simulate TCs such that the spatial patterns and frequencies of observed TCs are generally well-captured, as shown in the density maps provided in Figure 1. Simulated TCs are generated in all basins with observed TC activity with similar magnitudes to observed TC frequencies. In addition, the highest densities of observed TC activity (which occur in the Western and Eastern Pacific basins) are accurately reproduced by GCMs. However, some model bias in TC spatial distribution and frequency is evident. All GCMs generate TCs more frequently than observed in the Western Pacific and Indian Ocean basins, while AM2.5 and FLOR feature a negative bias over the far Eastern Pacific and a positive equatorward bias in simulated TCs in the Western Pacific. Moreover, FLOR features a positive bias in TC frequency over the Central Pacific and a slight negative bias for the northern extent of North Atlantic TC activity.

The intensity distributions of TC lifetime maximum intensity (LMI) for observed and simulated TCs are provided in Figure 2, with maximum 10 m wind speed (Figure 2a) and minimum sea-level pressure (Figure 2b) used as metrics for intensity. Regarding wind speed, observed TCs have a higher median maximum 10 m wind speed than

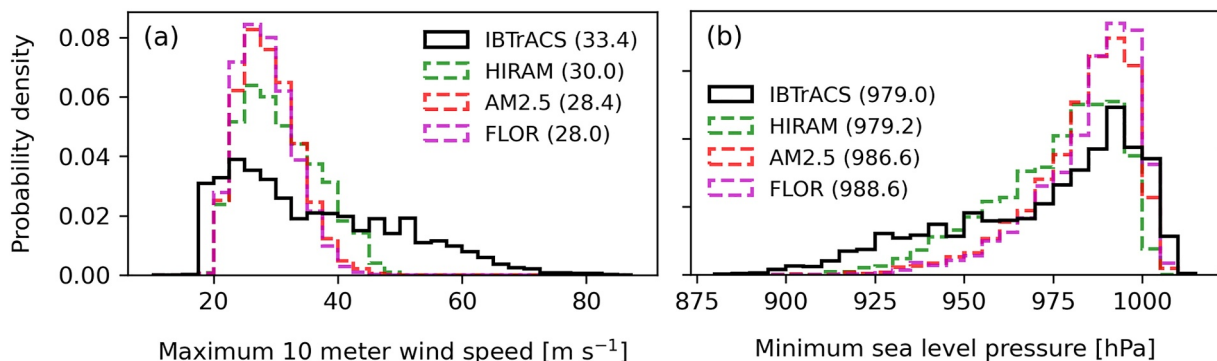


Figure 2. Comparison of lifetime maximum intensity (LMI) probability density functions between observed best-track (IBTrACS) and simulated TCs from control configurations of the GCMs used in this study (HiRAM, AM2.5, FLOR), as measured by panel (a) maximum 10 m wind speed and (b) minimum sea-level pressure. Parenthetical values in the figure legends denote median values of the intensity distribution for the corresponding TC data set.

the simulated TCs in all GCMs, as well as a broader intensity range due to the presence of strong TCs in the observed TC data set. Regarding minimum sea-level pressure, simulated TCs capture the distribution of minimum observed TC pressures more closely than 10 m wind speed, despite observed median minimum sea-level pressures being lower than all GCMs. The relatively stronger and broader intensity distributions in observed TCs are expected given the coarse resolution afforded by the GCMs relative to best-track data (spatial resolution of approximately 0.5°), which aligns with results from a similar analysis performed in Wing et al. (2019).

2.4. Tropical Cyclone Tracking

To track TCs in the suite of GCMs used herein, we use the algorithm presented in Harris et al. (2016). In this algorithm, vortices are tracked on a 6 hr temporal basis using sea-level pressure, horizontal anomalies of 200–350 hPa temperature to identify a warm-core system, 10 m horizontal wind speeds, and 850 hPa relative vorticity exceeding a magnitude of $1.5 \times 10^{-4} \text{ s}^{-1}$. Vortices satisfying these criteria are then tracked over time, with a longevity threshold of 3 consecutive days (72 hr) that must be met for an atmospheric disturbance to qualify as a TC. More details regarding the algorithm can be found in the appendix of Harris et al. (2016).

Several terms used throughout the study will be defined here. The term “tropical cyclones” (TCs) refers to vortices in GCMs that possess TC-like features. Using the aforementioned tracking methodology, TCs are defined as systems that meet the tracking criteria and feature maximum 10 m wind speeds that exceed 17.5 m s^{-1} , with TCs being classified as hurricane-strength when maximum 10 m wind speeds meet or exceed 33 m s^{-1} (Murakami et al., 2016). When referring to portions of TCs, the term “inner-core” generally refers to the radial extent of the TC with winds exceeding 15 m s^{-1} , although this term is more qualitatively used to identify portions of TCs with classical TC-like characteristics near the center (e.g., strong ascent, high precipitation rates, large vertical extent of near-saturated air). Correspondingly, the term “outer core” refers to the radial extent of the TC where these characteristics are not generally observed, but still falls within the wind field attributable to the TC. Finally, the term “far-field” refers to the portion of the domain near TCs that are not directly influenced by the TC circulation.

2.5. Potential Intensity Theory

The impacts of SWISHE on TC intensity can be interpreted using potential intensity (PI) theory, as developed in K. A. Emanuel (1986). F. Zhang and Emanuel (2016) expanded on this theory by deriving an expression for the theoretical 10 m wind speed attainable by a TC with surface enthalpy fluxes derived using capped wind speeds (V_{cap}), thus limiting surface enthalpy fluxes. As derived in F. Zhang and Emanuel (2016), the maximum wind speed attainable using PI theory, V_{max} , is expressed as:

$$V_{\text{max}} = V_{\text{cap}}^{1/3} V_{\text{pot}}^{2/3} \quad (2)$$

where V_{pot} is the PI maximum wind speed. Per Section 2.1, the capped wind speed used for surface enthalpy fluxes in this study is set to 0 m s^{-1} when 10 m wind speeds exceed 15 m s^{-1} and $n \geq 2.5$.

To analyze the relationship between simulated TCs and PI, PI is derived from the GCM runs performed using the methodology provided in Bister and Emanuel (2002). A monthly climatology of PI in GCMs is derived using monthly averaged values of SST, sea-level pressure, vertical temperature profiles, and vertical specific humidity profiles. Once a monthly climatology of PI is generated over the duration of each GCM run, the PI for a simulated TC is obtained. Obtaining the PI for a TC enables a comparison to be made between the maximum simulated intensity and the PI of the TC. To obtain PI for a given TC, the date and location LMI of a given TC is obtained, which are then used to index the PI for the LMI location during the month in which LMI occurs. To ensure PI analysis is applied to classical TCs (i.e., of tropical origin), TCs used for PI analysis must experience LMI within TC-active basins, as determined by IBTrACS documentation and specified in Schreck et al. (2014).

2.6. Composite Analysis

Compositing analysis is used in this study to evaluate the impact of SWISHE on surface fluxes by comparing the composite mean latent and sensible heat fluxes in control and SWISHE TCs.

Planar composite means of TCs are generated by:

1. Using the TC tracker outlined by Harris et al. (2016) to locate a given TC in the corresponding GCM run in time and space,
2. Identifying the exact TC center using minimum sea-level pressure,
3. Clipping a spatial extent of the domain surrounding the TC center from GCM output data, and
4. Selecting a subset of the data using a given pressure level and environmental field of interest

After data from all identified TCs has been extracted, the data is compiled and averaged to obtain a planar composite mean.

Due to the anticipated difference in intensity distributions between control and SWISHE TCs (i.e., control TCs are expected to be stronger than SWISHE TCs), the comparison of composite TC properties between experiments risks overrepresenting the composite mean difference between data sets. As an example, consider the comparison of surface fluxes between control and SWISHE TCs; surface fluxes are a function of wind speed, and control TCs are anticipated to feature a stronger median wind speed than SWISHE TCs. Therefore, it may become difficult to know if the composite mean difference in surface fluxes is due to the suppression of LHF by SWISHE, or a function of some different mechanism. To address this risk, TCs are sampled over an intensity range common to both experiments. In other words, a TC is used for composite analysis if its intensity falls within a range that features a sufficient number of TCs in both experiments.

The common intensity range used for sampling TCs for composite analysis is a maximum wind speed between 17 and 33 m s^{-1} , as the majority of both control and SWISHE TCs feature LMIs in this range; the rationale for this selection is discussed further in Section 3.

For each composite mean generated, a minimum of 100 TCs (to ensure TC diversity) and a minimum of 2,500 individual TC snapshots (i.e., instantaneous TC field values, to ensure a large sample size) are obtained for each model-experiment configuration. To address the potential for spatial biases introduced by sampling from different TC-active basins, TCs are selected at a frequency proportional to basin TC activity, such that the subset of TCs is representative of the global distribution of TCs (e.g., the Western Pacific basin has higher TC activity than the North Indian basin, Therefore more TCs are sampled from the Western Pacific than the North Indian). The statistical significance of composite mean differences is obtained using 10,000 bootstrap estimates of the differences between control and SWISHE composite means (difference = SWISHE—control) at the 95% confidence interval.

3. Results

In the model runs performed, the SWISHE algorithm resulted in a TC frequency reduction of 41% for HiRAM, 50% for AM2.5, and 43% for FLOR over the entire TC intensity distribution. For TCs of hurricane-strength intensity, the sensitivity to SWISHE is large: TC frequency was reduced by approximately 81% for HiRAM, 96% for AM2.5, and 95% for FLOR. The differential impact of SWISHE on all TCs and hurricane-strength TCs suggests that the feedback between wind and evaporation (i.e., WISHE) plays a secondary role in TC intensification during genesis. This is consistent with analyses of TC energetics at different states of TC development,

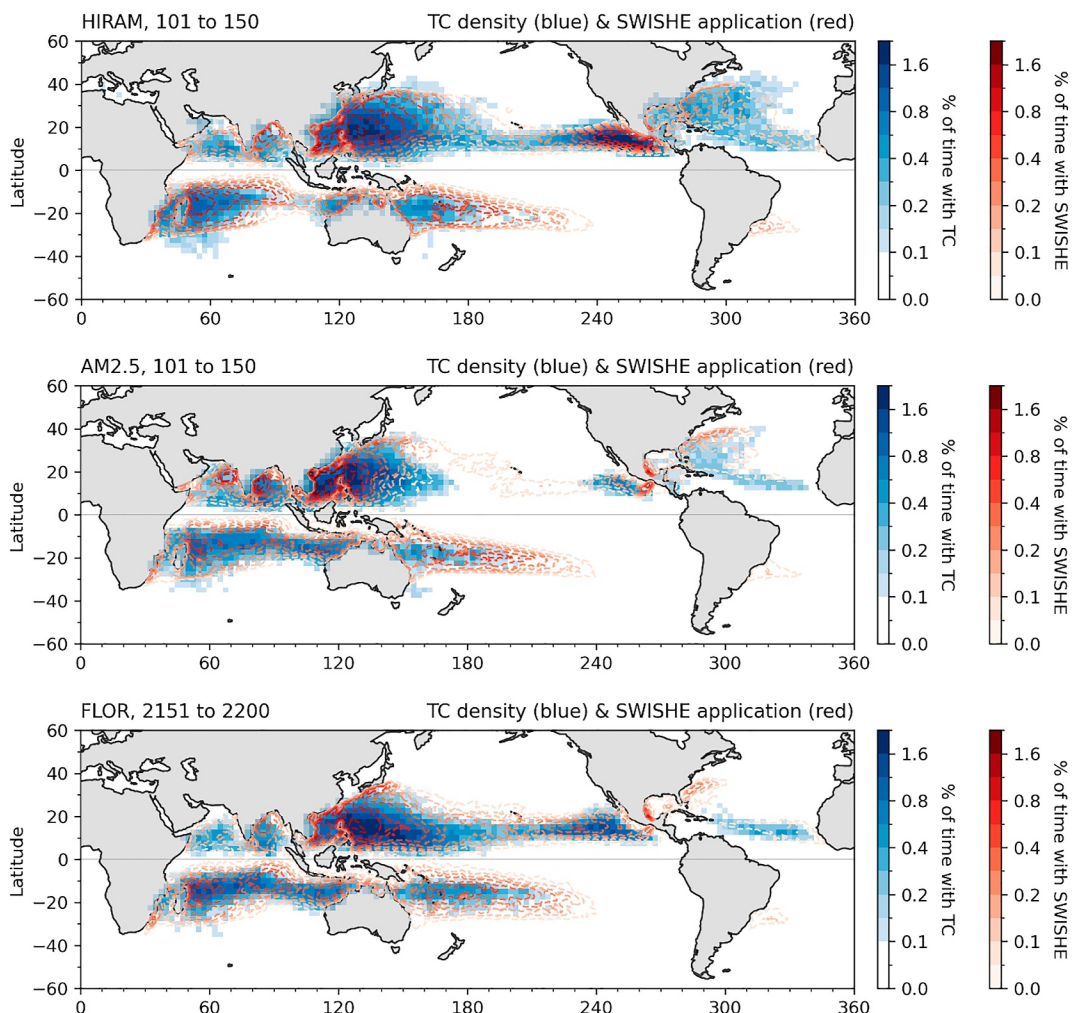


Figure 3. Temporal frequency of tropical cyclone (TC) occurrence (filled blue contours) and frequency of SWISHE algorithm application (open red contours) for HiRAM (top row), AM2.5 (center row), and FLOR (bottom row) over their respective 50-year run periods. Temporal frequency of TC occurrence is obtained from the control experiments of each GCM, while the frequency of SWISHE application is obtained from the SWISHE experiments of each GCM. Frequency is in units of per unit time (e.g., 1% frequency indicates a TC is present for a given grid cell 1 in every 100 days). Both sets of contours range from 0% to 1.6% and share common contour intervals.

indicating that processes such as radiative feedbacks and MSE convergence play a larger role in storm intensification than WISHE feedback for incipient TCs (Wing et al., 2019; B. Zhang et al., 2021). To understand the impact of this algorithm on modeled TC climatologies and storm-specific properties, this section will evaluate the implementation of the SWISHE algorithm on the suite of GCMs described in Section 2 in Section 3.1 and investigate the impacts of the SWISHE algorithm on aggregate TC properties (i.e., occurrence frequency, maximum intensity, composite analysis) in Section 3.2.

3.1. Algorithm Effectiveness

The goal of the SWISHE algorithm was to reduce TC frequency by targeting evaporation in TCs when winds are sufficiently strong to induce a WISHE feedback, while minimizing application of the frequency elsewhere. The application of SWISHE is visualized relative to the climatology of TC frequency in the GCMs used in Figure 3. The visualized metric is frequency of TC occurrence as a percentage of time (e.g., if a TC center is present over a model grid cell for 1 out of every 100 days, the corresponding percentage would be 1%). TC occurrence frequency in the control configuration of all GCMs is shown in the filled contours, while SWISHE application frequency is

Table 2

Number of TCs Detected for Each Model and Experiment Over a Run of 50 Model Years Grouped by Intensity Bins of Maximum Tropical Cyclone Intensity

Intensity bin	HiRAM		AM2.5		FLOR	
	Control	SWISHE	Control	SWISHE	Control	SWISHE
Number of TCs	5,256	3,161	3,969	1,991	4,381	2,504
Number of hurricane-strength TCs	2,374	450	1,381	58	1,342	73
% reduction, all TCs		40.0		49.8		42.9
% reduction, hurricane-strength TCs		81.0		95.8		94.6

Note. Reductions of TC frequency in SWISHE relative to control by intensity category are in percentage units, while the totals are absolute counts. Note that the data does not reflect the total number of storms used for the composite analyses in Section 3.

shown in the open contours. All models exhibit good agreement between TC occurrence frequency and SWISHE application frequency.

The spatial extent of SWISHE application roughly spans the spatial extent of modeled climatological TC activity for all models, although there are several basins in which spatial discrepancies occur. Storm activity in all TC basins where TCs are observed is identified by the SWISHE algorithm, with the spatial extents of SWISHE algorithm application varying with locations of model-specific climatological TC activity. However, the SWISHE algorithm does not adequately identify TC activity in the central-western North Pacific for the atmosphere-only models, fails to capture TC activity in portions of the Arabian Sea in AM2.5 and FLOR, and underdetects TC activity in the central North Atlantic basin in all models. Critically, SWISHE does not appear to target areas without TC activity, providing evidence to show that this algorithm is only suppressing evaporation for TCs and ignoring similar atmospheric phenomena. The climatological SWISHE application frequency matches climatological TC activity well. In other words, the locations of highest SWISHE application frequency coincide with the locations of the highest modeled climatological TC frequencies. For example, SWISHE application frequency contour values are highest over the western North Pacific and southwestern Indian Ocean for all models, which coincides with the high density of TC activity in the model output. As encountered in the evaluation of the spatial extent of the SWISHE algorithm, intermodel variability is present in the correlation of SWISHE application frequency and TC activity frequency. In HiRAM, SWISHE application frequency magnitude and spatial extent is approximately equivalent to the climatological TC frequency in the eastern North Pacific (approximately 1.6% for both frequencies), whereas SWISHE is applied much less frequently in AM2.5 and FLOR (maximum SWISHE application frequency of 1.0% and 0.6%, respectively) for the same basin. The ability of HiRAM to replicate the observational climatology of TC frequency more accurately than AM2.5 and FLOR is attributable to improved representation of deep convection in HiRAM, which is a function of differences in the convective scheme used in HiRAM versus the scheme used in AM2.5 and FLOR (Zhao et al., 2009). In contrast, the inability for SWISHE to represent TC activity in certain areas (e.g., Arabian Sea in FLOR, the eastern North Atlantic in all models, the western Central Pacific in HiRAM) cannot be attributed to a single reason and is a feature that requires further investigation. Despite the discrepancies between modeled TC activity and SWISHE application, the spatiotemporal coherence between climatological TC activity and SWISHE application frequency provides confidence that the algorithm is effectively targeting TCs and therefore suitable for exploring the motivating question.

Table 2 provides statistics for TC activity in each model configuration (control and SWISHE) over their respective run durations of 50 model years. TC activity is decomposed into intensity categories of all TCs and hurricane-strength TCs, as well as intensity bin percentages to contrast the intensity distributions for the control and SWISHE configuration runs. Over the model runs analyzed, a minimum of approximately 4,000 individual TCs were identified for each run in the control configuration, corresponding to an average of approximately 80 TCs worldwide per year, at minimum. Of these TCs, approximately 30%–45% reached hurricane-strength, depending on the model. Of the models used, HiRAM produced the highest number of TCs (approximately 105 TCs per year, globally) and featured the highest number of hurricane-strength TCs (approximately 47 TCs per year, globally), which exceeds the TC frequencies in AM2.5 and FLOR. The discrepancy in TC intensity distributions is attributable to a modified convective scheme in HiRAM relative to AM2.5 and FLOR resulting in

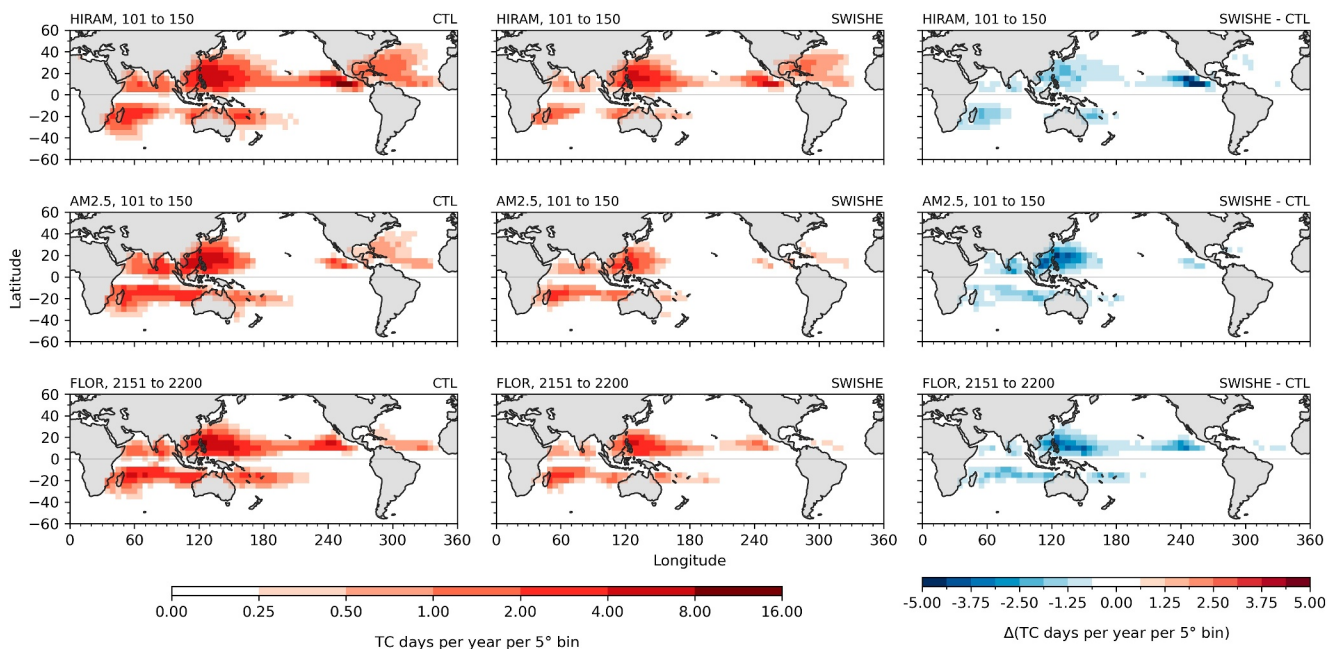


Figure 4. Density maps of tropical cyclone (TC) locations for TCs of all intensities. Density is calculated per model grid cell by the number of days experiencing a TC per year, grouped by $5^\circ \times 5^\circ$ spatial bins. Rows indicate different climate models and columns indicate the model configuration (control and SWISHE), and the difference (SWISHE—control).

global TC frequencies closely matching that of the observed climatology, as mentioned in Section 2 and discussed extensively in Zhao et al. (2009). The number of all TCs is reduced in the SWISHE configuration relative to the control for all models, but the largest reductions occur for hurricane-strength TCs; all TC activity is reduced by a model-aggregate mean of 44% from control to SWISHE model configurations, while TC activity for storms of hurricane-strength is reduced by an aggregate mean of 90%, as shown in Table 2.

In addition to the main set of runs evaluated in this study with only LHF suppressed, an exploratory study was performed in which LHF and SHF are both suppressed using an extension of the method described in Section 2.1. This set of model integrations intends to explore the limitation of enthalpy exchange as performed in F. Zhang and Emanuel (2016). The exploratory model runs were performed using only AM2.5 integrated for 25 model years. Preliminary results from the exploratory run yield a reduction in TC frequency of approximately 75% relative to control, with a reduction in frequency of hurricane-strength TCs of approximately 95%. These results indicate that the suppression of SHF in addition to LHF results in a TC suppression algorithm that is considerably more effective than LHF alone and merits additional exploration in future studies.

3.2. SWISHE Impacts on Aggregate TC Properties

To understand the impact of SWISHE on TC properties, this section will investigate the impacts of the algorithm on the frequency and spatial distribution of TC activity (Section 3.2.1), analyze the impact of SWISHE on TC intensity distributions (Section 3.2.2), interpret the impacts of SWISHE on TC intensity using the PI theoretical framework (Section 3.2.3), and determine the effects of SWISHE on surface fluxes using composite analysis of TCs (Section 3.2.4).

3.2.1. Impacts of SWISHE on TC Frequency and Spatial Distribution

To evaluate the impacts of SWISHE on the spatial distribution of TC frequency, Figures 4 and 5 present the climatologies of TC occurrence globally for each GCM and configuration used. The climatology of all TCs is presented in Figure 4, while the subset of the climatology pertaining to hurricane-strength TCs is presented in Figure 5. The difference between TC activity climatologies in the control and SWISHE configurations is presented in the rightmost column of Figures 4 and 5 (SWISHE—control) to emphasize the impact of the SWISHE algorithm on the frequency of TC occurrence in the GCMs used for this study.

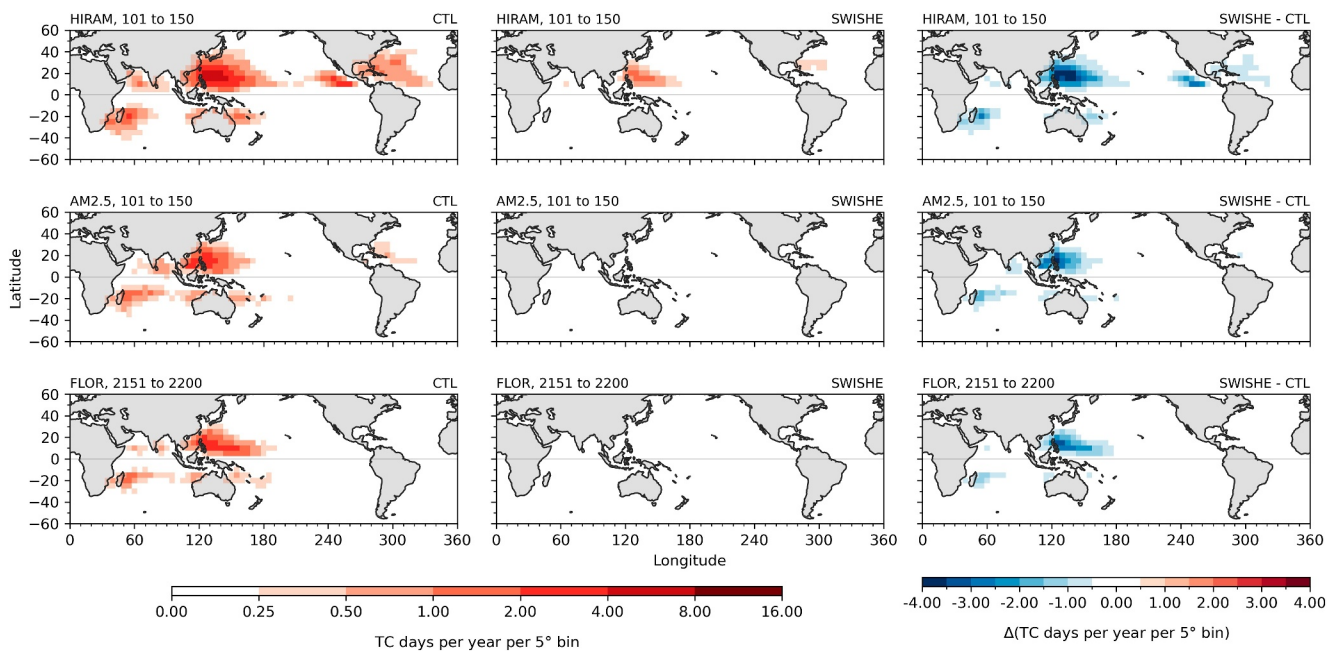


Figure 5. As in Figure 4 for hurricane-strength TCs.

TC activity locations and frequencies in the GCMs used for this study correspond to observed climatologies of TC activity and frequency. TC activity is modeled in all basins where TC activity is observed, with basins of high TC frequency (e.g., western North Pacific, southern Indian Ocean, far eastern North Pacific) corresponding to basins where the highest TC frequencies are observed. Despite the correspondence between modeled and observed TC climatologies, intermodel variability in climatological TC location and frequency is exhibited among the suite of GCMs used herein. In the HiRAM control run, TC activity is present in all basins where TCs are observed to occur, with highest frequencies occurring in the western and eastern North Pacific basins. HiRAM also produces TCs in the central northern Pacific, with TC activity occurring along the band from 5 to 15°N across the entire Pacific. This phenomenon has been noted in analyses of TC activity using the FLOR model (Vecchi et al., 2014; W. Zhang et al., 2016). For AM2.5, TC activity is present in all basins where observed TCs occur, with highest frequencies in the western North Pacific basin and the southern Indian Ocean. However, AM2.5 does not fully capture TC frequency in the eastern North Pacific and North Atlantic basins to the degree that HiRAM does. Despite sharing an atmospheric model with AM2.5, FLOR produces a spatial pattern of TC activity similar to HiRAM, with the highest TC frequencies occurring in the western and eastern North Pacific basins, respectively, and a pronounced band of TC activity in the low latitudes across the central north Pacific. The bias of GFDL models to preferentially simulate TC activity in the Pacific compared to the Atlantic has been documented in several studies (Chen & Lin, 2011; Vecchi et al., 2014; Zhao et al., 2009). Note that this bias is not considered to influence the results of this study given the storm-centric and model-based, rather than observational, nature of the analysis. Additionally, note that a notable difference in the climatological extent and frequency of TC activity between AM2.5 and FLOR exists, despite possessing the same atmospheric models, albeit with different oceanic boundary conditions. The difference in TC climatologies highlights the role of an interactive oceanic boundary condition on the representation of TCs in GCMs.

As mentioned at the beginning of Section 3, TC frequencies were reduced by 41% for HiRAM, 50% for AM2.5, and 43% for FLOR in the SWISHE runs relative to TC frequencies in the control runs, respectively. As shown in Figure 4, the number of days per year where TCs are detected for a given $5^\circ \times 5^\circ$ model grid cell decrease for almost all cells, indicating a global reduction in TC occurrence. Reductions in TC frequency appear to be proportional to the TC frequency, given that the strongest reductions in TC frequency occur for grid cells where TC frequency is greatest (typically the western North Pacific, southwestern Indian Ocean and the far eastern North Pacific). Despite global reductions in TC activity, a large number of TCs remain in the SWISHE configuration

runs, with several model grid cells experiencing upwards of 5 TC days per year, especially in the basins where TC activity is highest.

In contrast, hurricane-strength TCs are almost entirely suppressed (see Figure 5). As previously mentioned, for TCs of hurricanes-strength intensities, TC frequency was reduced by 82% for HiRAM, 96% for AM2.5, and 95% for FLOR. In AM2.5 and FLOR model runs, no grid cells experience more than 0.38 TC days per year, while for HiRAM, no model grid cell experiences more than 1.12 TC days per year. The discrepancy in the resolution of hurricane-strength TCs is attributable to the differences in convective parameterizations in AM2.5 and FLOR from the parameterization in HiRAM, as discussed in Section 2, which enables HiRAM to produce more intense TCs despite having the same spatial resolution as AM2.5 and FLOR. The climatological locations of TC genesis and lifetime maximum intensity in the SWISHE configuration are not significantly different from those in the control configuration. Maximum shifts in the latitude of peak TC genesis frequency were approximately 2°, with negligible shifts in the zonal distribution of TC activity.

3.2.2. Impacts of SWISHE on TC Intensity

To evaluate the effect of the SWISHE algorithm on the intensity of TCs in GCMs, probability distributions of maximum 10 m horizontal wind speed and minimum sea level pressure are provided in Figure 6 for all identified TCs in the control and SWISHE configurations for all models.

In the probability distributions of 10 m horizontal wind speed shown in Figures 6a–6c, the SWISHE configuration shows a marked reduction in distribution extent and median LMI wind value relative to the control configuration for all models. The control run distributions span from approximately 12 to 50 m s⁻¹ depending on the model, indicating that incipient and hurricane-strength TCs alike are accounted for in these runs. In contrast, the SWISHE run distributions span from approximately 12 to 40 m s⁻¹, indicating that the SWISHE configuration fails to reproduce the strongest TCs observed in the control run, despite still allowing some low-end hurricane-strength storms to form. Median wind speed values decrease from their control to their SWISHE configurations by 4.1 m s⁻¹ (29.9–25.8 m s⁻¹), 4.2 m s⁻¹ (28.6–24.4 m s⁻¹), and 3.5 m s⁻¹ (27.9–24.4 m s⁻¹) for HiRAM, AM2.5, and FLOR, respectively. Moreover, all models experience reductions in the standard deviations of their distributions, confirming the decrease in the variance of maximum winds exhibited by TCs in the SWISHE configuration. The maximum wind speed distributions of SWISHE TCs for all models share interquartile ranges ranging from 17 m s⁻¹ (largest intermodel 10% quantile) and 33 m s⁻¹ (smallest intermodel 90% quantile), which provides the intensity range used in the selection of TCs for composite analysis, as described in Section 2.6.

A similar finding is shown in Figures 6d–6f for minimum sea level pressure, as a comparison of control and SWISHE model runs shows a reduction in distribution extent and an increase in distribution medians from the control run to the SWISHE runs for all models. The control run distributions of minimum sea level pressure span from approximately 1,010 to 900 hPa across all models, further confirming that incipient and hurricane-strength TCs alike are accounted for in these runs. In comparison, the SWISHE run distributions span from approximately 1,010 to 940 hPa across all models, verifying that the SWISHE configuration does not produce TCs as intense as those in the control configuration. As found in the comparison of distributions of maximum 10 m wind speeds between control and SWISHE runs, the changes in distribution medians indicate a weakening in the distribution of minimum sea level pressures, as the median values increase by 6.1, 5.2, and 2.8 hPa for HiRAM, AM2.5, and FLOR, respectively. Similarly, all models experience notable reductions in standard intensity spread of SWISHE TCs.

Therefore, the decrease in distribution variance (i.e., a “thinning” of the distribution shape) is indicative of the energetic limit imposed by SWISHE on surface enthalpy fluxes, such that TC intensity is capped to a smaller (and weaker) intensity range when fluxes are capped. A subtle, yet interesting, trend appears when comparing changes to intensity distributions between runs from the fixed-SST GCMs (HiRAM and AM2.5) and the coupled GCM (FLOR); the decreases in median intensity with SWISHE are smaller when the ocean is allowed to respond to the atmospheric model. This is shown by smaller reductions in maximum 10 m wind and smaller increases in minimum sea level pressure in FLOR relative to HiRAM and AM2.5.

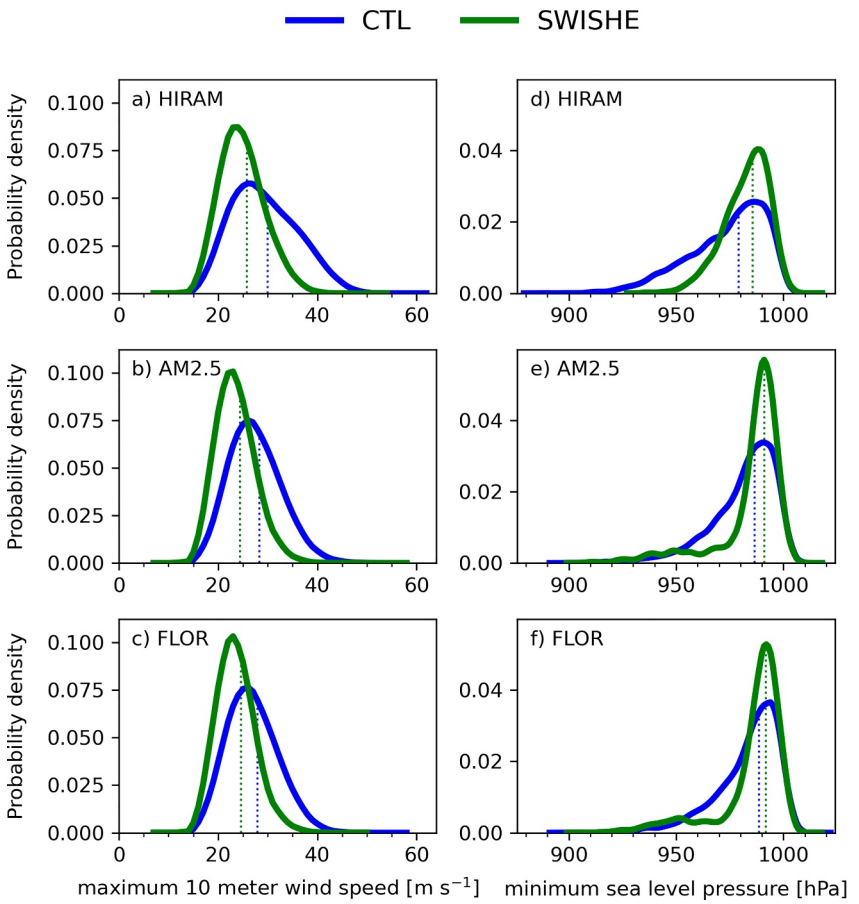


Figure 6. Probability density functions of tropical cyclone (TC) intensity using maximum TC 10 m wind speed (left column, panels a–c) and minimum TC sea level pressure (right column, panels d–f). Dashed vertical lines denote median values for the intensity distribution of each configuration. Note that the experiment named “CTL” corresponds to the control configuration and the experiment named “SWISHE” corresponds to the SWISHE, or experimental, configuration.

3.2.3. Interpreting SWISHE Results Using Potential Intensity Theory

Using the methodology of Section 2.5, a comparison of simulated TC intensities at LMI for both control and SWISHE configurations is provided in Figure 7. The maximum 10 m wind speeds for tracked TCs at LMI in GCMs are shown relative to theoretical limits obtained from PI theory for theoretical maximum wind speed limits when surface enthalpy fluxes are derived using uncapped (dotted curve) and capped wind speeds (dashed curve, following Equation 2). For simulated TCs in the control configuration, the maximum 10 m wind speeds at LMI (blue circles) are almost entirely below the theoretical maximum wind speed (V_{pot}) for all GCMs, indicating that PI is an effective metric of maximum possible TC intensity in the GCMs used herein. Accordingly, almost all simulated TCs in the SWISHE configuration feature LMI maximum 10 m wind speeds below V_{max} , further demonstrating that PI theory accurately establishes a limit for simulated TC intensity, with the extensions to PI theory derived in F. Zhang and Emanuel (2016) incorporated. Despite intermodel differences (e.g., HiRAM features more instances of TCs exceeding their respective theoretical intensity limits), this analysis demonstrates the utility of PI theory in determining an upper intensity bound, thus serving as a simple but effective intensity prediction method.

Note that several TCs from the SWISHE configuration (i.e., wind speeds used for calculating LHF are capped) exceed the theoretical V_{max} with capped wind speeds. This is attributable to two main causes in this study; the quantities for which winds speeds are capped, and the methodology used for obtaining PI for a given tracked TC. Regarding the capping of wind speeds, the derivation in F. Zhang and Emanuel (2016) caps wind speeds for the total surface enthalpy flux, whereas SWISHE does so only for LHF. Given that SWISHE places a less stringent

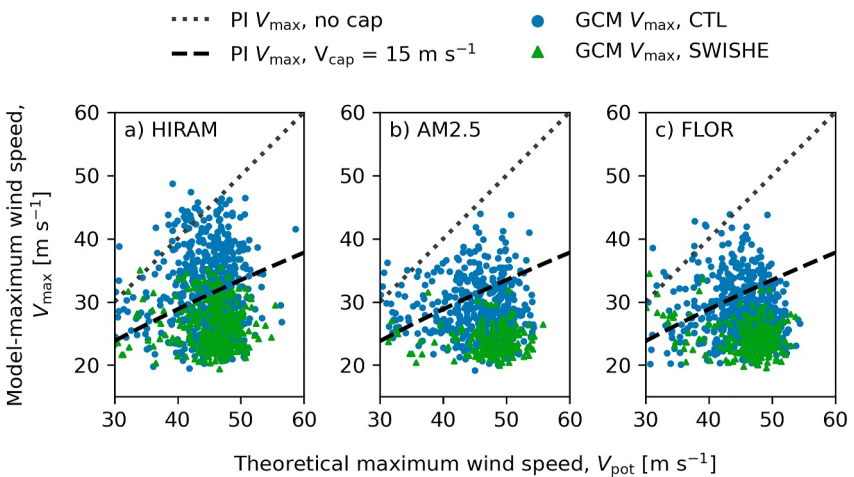


Figure 7. Comparison of lifetime maximum intensities (LMI) of TCs from control and SWISHE configurations (points) with theoretical intensity limits (curves). LMI for control and SWISHE configurations are shown in blue circles and green triangles, respectively, for TCs simulated in HIRAM (panel a), AM2.5 (panel b), and FLOR (panel c). Each point corresponds to an individual simulated TC. Theoretical maximum wind speed (V_{pot}), as dictated by potential intensity theory, is denoted by the dotted line. Theoretical maximum wind speed for TCs with suppressed wind speeds after exceeding the capped-wind threshold (V_{cap}) is denoted by the dashed line, which is generated using the theoretical limit in Equation 2.

cap on surface enthalpy fluxes, the resultant TC may intensify beyond the theoretical limit estimated by V_{max} for capped winds, due to processes such as sensible heating (see Section 4 for a brief discussion of sensible heat fluxes and TCs). Regarding the methodology used for obtaining PI for a given TC, we discuss the derivation of PI in Section 2.5, which is performed using monthly mean values of large-scale environmental properties, whereas TCs are tracked every 6 hr. Therefore, transient environmental conditions associated with TC activity (e.g., high specific humidity, large boundary layer enthalpy gradients) may not be captured by long-term time mean properties, especially outside of the tropics, where PI is climatologically high.

3.2.4. Surface Flux Composites

Figures 8 and 9 feature planar composites of surface latent heat and sensible heat fluxes for all models and configurations, with latent heat fluxes shown in Figure 8 and sensible heat fluxes in Figure 9. As expected, maximum composite mean LHF occurs in the TC inner core where winds are strongest in control TCs. In composite means of TCs sampled from models run in the control configuration, maximum LHF values range from approximately 200 to 240 W m^{-2} , with AM2.5 featuring the highest LHF and HiRAM featuring the lowest (see Figure 8). In contrast, composite mean LHF of TCs sampled from the SWISHE configurations of model runs experience their minima at the TC inner core. This is by design, as the suppression of WISHE results in highly limited evaporation where high winds occur. Minimum composite mean LHF in the SWISHE runs ranges from approximately 40 W m^{-2} in AM2.5–50 W m^{-2} in HiRAM. The robust suppression of LHF in TC inner cores is highlighted in the differences obtained between SWISHE and control composite means, as shown in Figure 8. All models exhibit statistically significant decreases in LHF due to the imposition of SWISHE, confirming the effectiveness of the algorithm on restricting surface fluxes where TC-like conditions occur.

The reductions in inner core LHF are partially offset by increases in inner core SHF for all models. In the control configuration, the maximum composite mean SHF ranges from 15 to 25 W m^{-2} , with highest fluxes occurring near the center (again, in areas with maximum horizontal wind speeds). In the SWISHE configuration, all models exhibit an increase in maximum composite mean SHF, with values ranging from 30 to 35 W m^{-2} . The increases in SHF from the control to the SWISHE composite means are an order of magnitude smaller than the decreases in LHF, indicating that the increase in sensible heating cannot fully offset the suppression of LHF due to SWISHE. Outside the inner core, the fixed SST models experience little changes to composite mean SHF, which contrasts with modest decreases (less than 7.5 W m^{-2}) encountered in the domain far-field in FLOR. The discrepancy in the responses may be attributable to the interactive oceanic boundary condition in FLOR, which is able to respond to

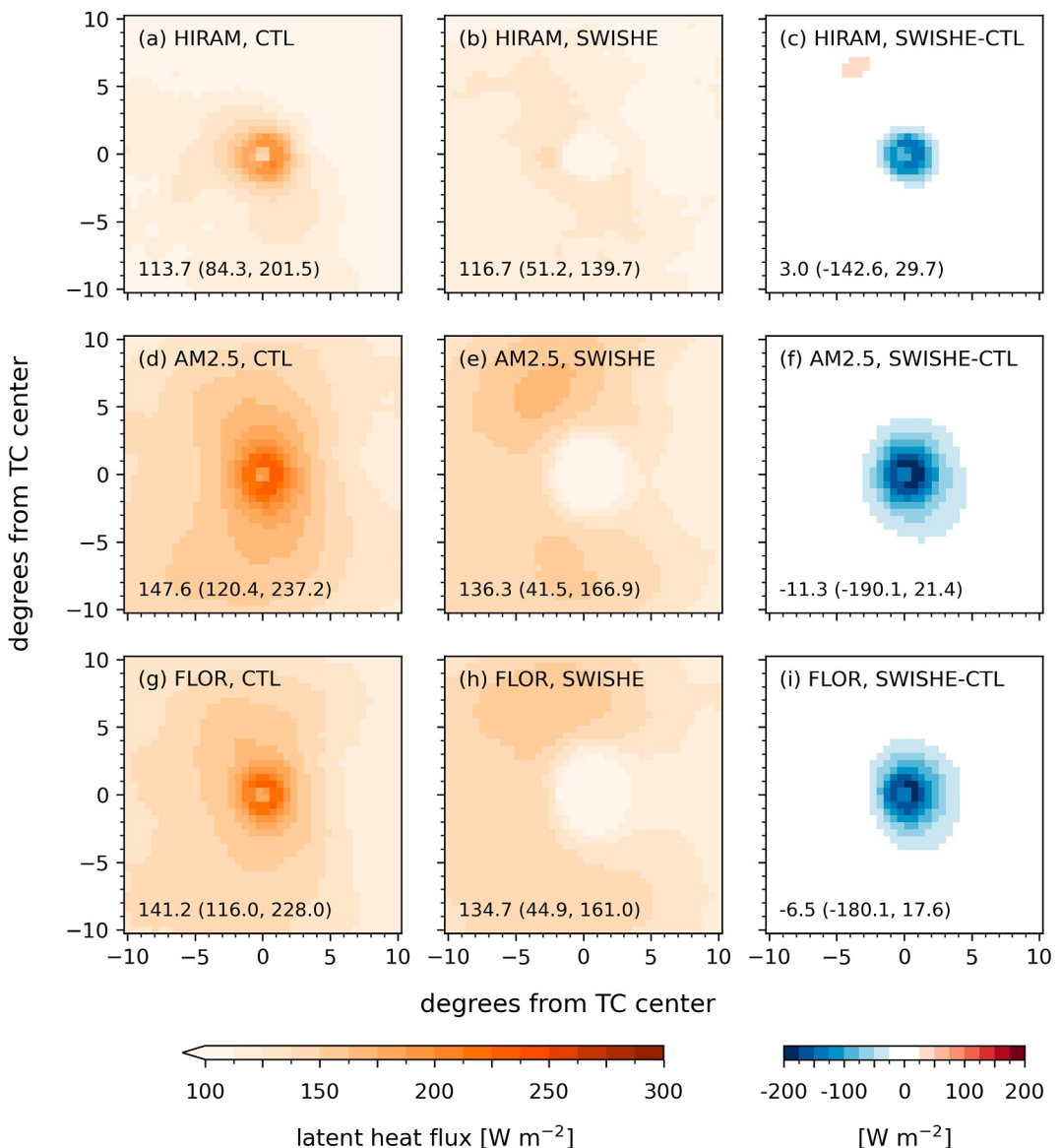


Figure 8. Planar composite means of latent heat flux (LHF) for TCs in control and SWISHE configurations. TCs used to generate composite means are obtained with intensities ranging from 17 to 33 m s⁻¹. Subplots (a, d, g) show the composite mean for control run TCs, (b, e, h) show the composite means for SWISHE TCs, and subplots (c, f, i) denote the mean difference. Annotations in the lower-left corner of the panels denote the domain average, domain minimum, and domain maximum values, respectively.

the increased size of TC wind fields in the SWISHE configuration. Wind-induced cooling from expanded wind fields may lower the air-sea temperature difference, resulting in lower SHF than a model with fixed SSTs.

4. Discussion and Conclusions

In this study, we introduced a novel algorithm to suppress tropical cyclones in a suite of GCMs and analyzed its impacts on TC frequency and properties.

We find that applying SWISHE resulted in 44% fewer TCs of all intensities and 90% fewer TCs of hurricane intensity over the suite of GCMs evaluated. The reduction in TC frequency in the SWISHE runs highlights the importance of latent heating for TC intensification in GCMs, especially for mature TCs with stronger wind speeds, where WISHE becomes dominant for TC intensification. Additionally, the inability of SWISHE to

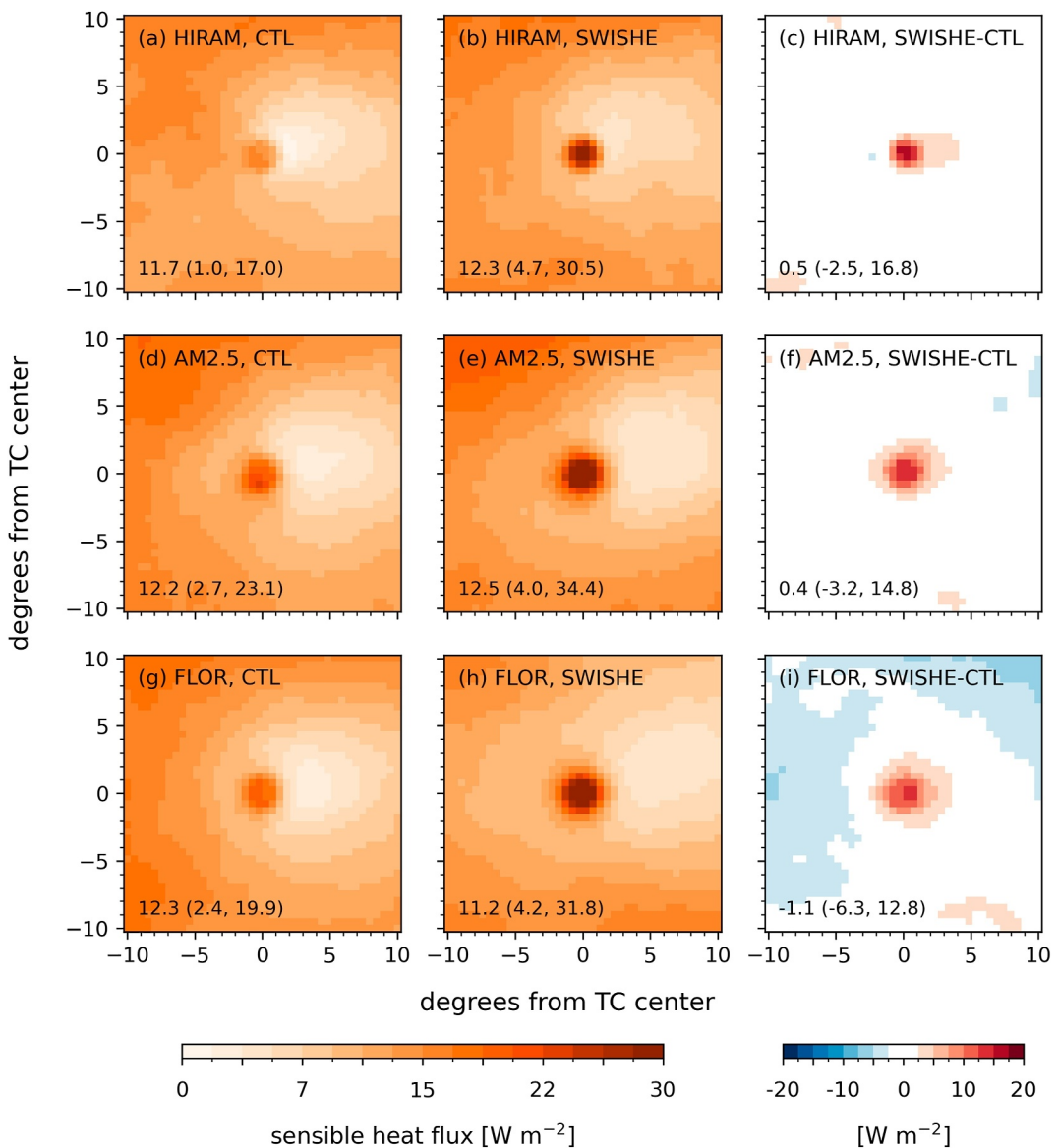


Figure 9. As in Figure 8 for sensible heat flux.

suppress a greater number of weaker (non-hurricane) TCs highlights the importance of other processes for TC formation (such as radiative interactions, see B. Zhang et al. (2021)).

We demonstrate the effectiveness of the SWISHE algorithm on reducing TC activity in several ways. First, we compare the location and frequency of SWISHE application to the location and frequency of the TC climatology in the GCMs evaluated, which is shown to align well in both aspects for all GCMs by Figure 3. Then, we compare TC frequencies in the control and SWISHE configurations as in Figures 4 and 5, which show substantial reductions in TC frequency for all storm intensities in the SWISHE configuration, with hurricane-strength TCs almost entirely suppressed for all model runs. TCs that form in the SWISHE configuration are weaker than control TCs, as median maximum 10 m wind speeds decrease and minimum sea-level pressures increase per Figure 6. Reducing scope from a global domain to a TC-centered domain, the effectiveness of SWISHE in suppressing LHF in TCs is evident in composite means presented in Figure 8, with a significant reduction in LHF in the inner cores of TCs, with little sensible heat compensation. Therefore, we have shown that the SWISHE algorithm effectively lowers TC frequency by arresting the development of TCs while minimizing the direct impact on other climate processes that depend on the wind-evaporation feedback. Although we show that composite mean SHF

values are far less than composite mean LHF values at TC inner cores, the preliminary results from model runs with both LHF and SHF suppression at grid cells with TC-like conditions, as compared to suppression of LHF alone in SWISHE, show further reductions in TC activity as discussed in Section 3.1. This provides evidence in the context of a GCM that SHF also contributes to TC intensification, as suggested in F. Zhang and Emanuel (2016), and paves the way for refinement of the SWISHE algorithm to further suppress TC activity in GCMs. In summary, the results shown herein further support the importance of WISHE on intensification in mature TCs (K. A. Emanuel, 1986; Rotunno & Emanuel, 1987; F. Zhang & Emanuel, 2016).

Several considerations should be taken when interpreting the methodology used in this study. First, we note that suppression of evaporation in TCs is inherently unphysical. Moreover, the method used to reduce TC frequency and weaken TC intensity is column-based, rather than being able to span several laterally across several grid cells for any given TC. This presents weaknesses in being unable to suppress evaporation for a larger spatial domain which may correspond to a detected TC, rather than the stringent conditions imposed for the SWISHE algorithm to avoid perturbing non-TC phenomena. However, this method presents an alternative path to exploring the climatic impact of TCs from previous methods of simulating reductions in TC activity. Ideally, improvements to this methodology would present a high-fidelity attempt at answering the question: “what if tropical cyclones were removed from the climate system entirely?” Second, the TCs generated in GCMs are weaker and less realistic than those simulated in numerical models with finer spatiotemporal resolutions (e.g., WRF, SAM). As a result, small-scale and transient processes that favor TC intensification aside from WISHE may not be addressed in this paper. Although the body of literature regarding the role of WISHE in TC development demonstrates it is critical to understanding the dominant processes in TC physics, we note that many findings in this body of literature involve processes that cannot be explicitly resolved by the GCMs used in this study (e.g., kilometer-scale deep convection, eyewall dynamics, extreme convective precipitation) and are therefore not explicitly addressed in this paper.

Despite these limitations, we note that GCMs provide quasi-realistic representations of TCs in the context of a large-scale environment, thus allowing the results presented to provide a first step toward improving the understanding of the remote impacts of TCs on the coupled climate system.

Data Availability Statement

The source code for CM2.5 is publicly available on the NOAA-GFDL website, at <https://www.gfdl.noaa.gov/cm2-5-and-flor-quickstart/>. The source code is modified in a separate repository to implement the SWISHE algorithm and can be found at Rios et al. (2025b). The model data used for this study are available on Zenodo repository via <https://doi.org/10.5281/zenodo.14623457> (Rios et al., 2025a). Resources for computing and data storage were provided by the Princeton Tiger computing cluster. This data is freely available for use via the Creative Commons Attribution license.

Acknowledgments

We thank Kerry Emanuel and two anonymous reviewers for helpful comments which greatly improved the quality of this manuscript. This material is based upon work supported by the U.S. Department of Energy, Office of Science, Office of Advanced Scientific Computing Research, Department of Energy Computational Science Graduate Fellowship (DOE CSGF) under award number DE-SC0024386. This material is also based on work supported by the Heising-Simons Foundation. The authors made significant use of Python packages xarray (Hoyer & Hamman, 2017) and Cartopy (Met Office, 2010 - 2015) and thank the developers for their efforts in making the software open-source.

References

- Bercos-Hickey, E., & Patricola, C. M. (2023). The effects of African easterly wave suppression by wave track on Atlantic tropical cyclones. *Geophysical Research Letters*, 50(23), e2023GL105491. <https://doi.org/10.1029/2023GL105491>
- Bister, M., & Emanuel, K. A. (2002). Low frequency variability of tropical cyclone potential intensity 2. Climatology for 1982–1995. *Journal of Geophysical Research*, 107(D22). <https://doi.org/10.1029/2001jd000780>
- Bretherton, C. S., McCaa, J. R., & Grenier, H. (2004). A new parameterization for shallow cumulus convection and its application to marine subtropical cloud-topped boundary layers. Part I: Description and 1D results. *Monthly Weather Review*, 132(4), 864–882. [https://doi.org/10.1175/1520-0493\(2004\)132<0864:ANPFSC>2.0.CO;2](https://doi.org/10.1175/1520-0493(2004)132<0864:ANPFSC>2.0.CO;2)
- Camargo, S. J., & Sobel, A. H. (2005). Western north pacific tropical cyclone intensity and ENSO. *Journal of Climate*, 18(15), 2996–3006. <https://doi.org/10.1175/jcli3457.1>
- Chen, J.-H., & Lin, S.-J. (2011). The remarkable predictability of inter-annual variability of Atlantic hurricanes during the past decade. *Geophysical Research Letters*, 38(11). <https://doi.org/10.1029/2011gl047629>
- Corbosiero, K. L., & Molinari, J. (2002). The effects of vertical wind shear on the distribution of convection in tropical cyclones. *Monthly Weather Review*, 130(8), 2110–2123. [https://doi.org/10.1175/1520-0493\(2002\)130<2110:teovws>2.0.co;2](https://doi.org/10.1175/1520-0493(2002)130<2110:teovws>2.0.co;2)
- Craig, G. C., & Gray, S. L. (1996). CISKE or WISHE as the mechanism for tropical cyclone intensification. *Journal of the Atmospheric Sciences*, 53(23), 3528–3540. [https://doi.org/10.1175/1520-0469\(1996\)053<3528:COWATM>2.0.CO;2](https://doi.org/10.1175/1520-0469(1996)053<3528:COWATM>2.0.CO;2)
- Cronin, T. W., & Chavas, D. R. (2019). Dry and semidry tropical cyclones. *Journal of the Atmospheric Sciences*, 2019(1), 1–20. <https://doi.org/10.1175/JAS-D-18-0357.1>
- Danso, D. K., Patricola, C. M., & Bercos-Hickey, E. (2022). Influence of African easterly wave suppression on Atlantic tropical cyclone activity in a convection-permitting model. *Geophysical Research Letters*, 49(22). <https://doi.org/10.1029/2022GL100590>
- Delworth, T. L., Broccoli, A. J., Rosati, A., Stouffer, R. J., Balaji, V., Beesley, J. A., et al. (2006). GFDL’s CM2 global coupled climate models. Part I: Formulation and simulation characteristics. *Journal of Climate*, 19(5), 643–674. <https://doi.org/10.1175/JCLI3629.1>

- Delworth, T. L., Rosati, A., Anderson, W., Adcroft, A. J., Balaji, V., Benson, R., et al. (2012). Simulated climate and climate change in the GFDL CM2.5 high-resolution coupled climate model. *Journal of Climate*, 25(8), 2755–2781. <https://doi.org/10.1175/JCLI-D-11-00316.1>
- Donnelly, J. P., & Woodruff, J. D. (2007). Intense hurricane activity over the past 5,000 years controlled by El Niño and the West African monsoon. *Nature*, 447(7143), 465–468. <https://doi.org/10.1038/nature05834>
- Emanuel, K. (2001). Contribution of tropical cyclones to meridional heat transport by the oceans. *Journal of Geophysical Research*, 106(D14), 14771–14781. <https://doi.org/10.1029/2000JD900641>
- Emanuel, K. (2008). The hurricane-climate connection. *Bulletin of the American Meteorological Society*, 89(5), ES10–ES14. <https://doi.org/10.1175/bams-89-5-emmanuel>
- Emanuel, K., DesAutels, C., Holloway, C., & Korty, R. (2004). Environmental control of tropical cyclone intensity. *Journal of the Atmospheric Sciences*, 61(7), 843–858. [https://doi.org/10.1175/1520-0469\(2004\)061<0843:ecotci>2.0.co;2](https://doi.org/10.1175/1520-0469(2004)061<0843:ecotci>2.0.co;2)
- Emanuel, K. A. (1986). An air-sea interaction theory for tropical cyclones. Part I: Steady-state maintenance. *Journal of the Atmospheric Sciences*, 43(6), 585–605. [https://doi.org/10.1175/1520-0469\(1986\)043\(0585:AASITF\)2.0.CO;2](https://doi.org/10.1175/1520-0469(1986)043(0585:AASITF)2.0.CO;2)
- Fisher, E. L. (1958). Hurricanes and the sea-surface temperature field. *Journal of Meteorology*, 15(3), 328–333. [https://doi.org/10.1175/1520-0469\(1958\)015\(0328:HATSSST\)2.0.CO;2](https://doi.org/10.1175/1520-0469(1958)015(0328:HATSSST)2.0.CO;2)
- Gangopadhyaya, M., & Riehl, H. (1959). Exchange of heat, moisture and momentum between Hurricane Ella (1958) and its environment. *Quarterly Journal of the Royal Meteorological Society*, 85(365), 278–286. <https://doi.org/10.1002/qj.49708536509>
- Gutiérrez Brizuela, N., Alford, M. H., Xie, S.-P., Sprintall, J., Voet, G., Warner, S. J., et al. (2023). Prolonged thermocline warming by near-inertial internal waves in the wakes of tropical cyclones. *Proceedings of the National Academy of Sciences*, 120(26), e2301664120. <https://doi.org/10.1073/pnas.2301664120>
- Harris, L. M., Lin, S.-J., & Tu, C. (2016). High-resolution climate simulations using GFDL HiRAM with a stretched global grid. *Journal of Climate*, 29(11), 4293–4314. <https://doi.org/10.1175/JCLI-D-15-0389.1>
- Hart, R. E., Maué, R. N., & Watson, M. C. (2007). Estimating local memory of tropical cyclones through MPI anomaly evolution. *Monthly Weather Review*, 135(12), 3990–4005. <https://doi.org/10.1175/2007MWR2038.1>
- Hazelworth, J. B. (1968). Water temperature variations resulting from hurricanes. *Journal of Geophysical Research*, 73(16), 5105–5123. <https://doi.org/10.1029/JB073i016p05105>
- Holt, B. (1976). *Some observations of ocean thermal response to typhoon passage*. (Tech. Rep.). Naval Postgraduate School.
- Hoyer, S., & Hamman, J. (2017). XARRAY: N-D labeled arrays and datasets in Python. *Journal of Open Research Software*, 5(1), 10. <https://doi.org/10.5334/jors.148>
- Hsieh, T.-L., Vecchi, G. A., Yang, W., Held, I. M., & Garner, S. T. (2020). Large-scale control on the frequency of tropical cyclones and seeds: A consistent relationship across a hierarchy of global atmospheric models. *Climate Dynamics*, 55(11), 3177–3196. <https://doi.org/10.1007/s00382-020-05446-5>
- Hu, L., Ritchie, E. A., & Scott Tyo, J. (2023). Quantifying the cooling effect of tropical cyclone clouds on the climate system. *npj Climate and Atmospheric Science*, 6(1), 99. <https://doi.org/10.1038/s41612-023-00433-z>
- Jacob, S. D., Shay, L. K., Mariano, A. J., & Black, P. G. (2000). The 3D oceanic mixed layer response to Hurricane Gilbert. *Journal of Physical Oceanography*, 30(6), 1407–1429. [https://doi.org/10.1175/1520-0485\(2000\)030\(1407:TOMLRT\)2.0.CO;2](https://doi.org/10.1175/1520-0485(2000)030(1407:TOMLRT)2.0.CO;2)
- Kim, D., Moon, Y., Camargo, S. J., Wing, A. A., Sobel, A. H., Murakami, H., et al. (2018). Process-oriented diagnosis of tropical cyclones in high-resolution GCMs. *Journal of Climate*, 31(5), 1685–1702. <https://doi.org/10.1175/JCLI-D-17-0269.1>
- Knapp, K. R., Kruk, M. C., Levinson, D. H., Diamond, H. J., & Neumann, C. J. (2010). The international best track archive for climate stewardship (IBTRACS) unifying tropical cyclone data. *Bulletin of the American Meteorological Society*, 91(3), 363–376. <https://doi.org/10.1175/2009bams2755.1>
- Knutson, T. R., McBride, J. L., Chan, J., Emanuel, K., Holland, G., Landsea, C., et al. (2010). Tropical cyclones and climate change. *Nature Geoscience*, 3(3), 157–163. <https://doi.org/10.1038/ngeo779>
- Leipper, D. F. (1967). Observed ocean conditions and Hurricane Hilda, 1964. *Journal of the Atmospheric Sciences*, 24(2), 182–186. [https://doi.org/10.1175/1520-0469\(1967\)024\(0182:OOCAHH\)2.0.CO;2](https://doi.org/10.1175/1520-0469(1967)024(0182:OOCAHH)2.0.CO;2)
- Lloyd, I. D., & Vecchi, G. A. (2011). Observational evidence for oceanic controls on hurricane intensity. *Journal of Climate*, 24(4), 1138–1153. <https://doi.org/10.1175/2010jcli3763.1>
- Ma, Z., & Fei, J. (2022). A comparison between moist and dry tropical cyclones: The low effectiveness of surface sensible heat flux in storm intensification. *Journal of the Atmospheric Sciences*, 79(1), 31–49. <https://doi.org/10.1175/JAS-D-21-0014.1>
- Manucharyan, G. E., Brierley, C. M., & Fedorov, A. V. (2011). Climate impacts of intermittent upper ocean mixing induced by tropical cyclones. *Journal of Geophysical Research*, 116(C11), 2011JC007295. <https://doi.org/10.1029/2011JC007295>
- McFadden, J. A. M. E. S. D. (1967). Sea-Surface temperatures in the wake of Hurricane Betsy (1965). *Monthly Weather Review*, 95(5), 299–302. [https://doi.org/10.1175/1520-0493\(1967\)095\(0299:SSTITW\)2.3.CO;2](https://doi.org/10.1175/1520-0493(1967)095(0299:SSTITW)2.3.CO;2)
- Met Office. (2010 - 2015). Cartopy: A cartographic python library with a matplotlib interface [Computer Software Manual]. Exeter, Devon. Retrieved from <https://scitools.org.uk/cartopy>
- Muller, C. J., & Romps, D. M. (2018). Acceleration of tropical cyclogenesis by self-aggregation feedbacks. *Proceedings of the National Academy of Sciences*, 115(12), 2930–2935. <https://doi.org/10.1073/pnas.1719967115>
- Murakami, H., Vecchi, G. A., Villarini, G., Delworth, T. L., Gudgel, R., Underwood, S., et al. (2016). Seasonal forecasts of major hurricanes and landfalling tropical cyclones using a high-resolution GFDL coupled climate model. *Journal of Climate*, 29(22), 7977–7989. <https://doi.org/10.1175/jcli-d-16-0233.1>
- Murthy, V. S., & Boos, W. R. (2018). Role of surface enthalpy fluxes in idealized simulations of tropical depression spinup. *Journal of the Atmospheric Sciences*, 75(6), 1811–1831. <https://doi.org/10.1175/JAS-D-17-0119.1>
- O'Brien, J. J., & Reid, R. O. (1967). The non-linear response of a two-layer, baroclinic ocean to a stationary, axially-symmetric hurricane: Part I. Upwelling induced by momentum transfer. *Journal of the Atmospheric Sciences*, 24(2), 197–207. [https://doi.org/10.1175/1520-0469\(1967\)024\(0197:TNLROA\)2.0.CO;2](https://doi.org/10.1175/1520-0469(1967)024(0197:TNLROA)2.0.CO;2)
- Patricola, C. M., Chang, P., & Saravanan, R. (2016). Degree of simulated suppression of Atlantic tropical cyclones modulated by flavour of El Niño. *Nature Geoscience*, 9(2), 155–160. <https://doi.org/10.1038/ngeo2624>
- Peng, C.-H., & Wu, C.-C. (2020). The impact of outer-core surface heat fluxes on the convective activities and rapid intensification of tropical cyclones. *Journal of the Atmospheric Sciences*, 77(11), 3907–3927. <https://doi.org/10.1175/JAS-D-19-0348.1>
- Pérez-Alarcón, A., Coll-Hidalgo, P., Fernández-Alvarez, J. C., Trigo, R. M., Nieto, R., & Gimeno, L. (2023). Impacts of tropical cyclones on the global water budget. *npj Climate and Atmospheric Science*, 6(1), 212. <https://doi.org/10.1038/s41612-023-00546-5>
- Price, J. F. (1981). Upper Ocean response to a hurricane. *Journal of Physical Oceanography*, 11(2), 153–175. [https://doi.org/10.1175/1520-0485\(1981\)011\(0153:UORTAH\)2.0.CO;2](https://doi.org/10.1175/1520-0485(1981)011(0153:UORTAH)2.0.CO;2)

- Rayner, N., Parker, D. E., Horton, E., Folland, C. K., Alexander, L. V., Rowell, D., et al. (2003). Global analyses of sea surface temperature, sea ice, and night marine air temperature since the late nineteenth century. *Journal of Geophysical Research*, 108(D14). <https://doi.org/10.1029/2002jd002670>
- Reed, K. A., Wehner, M. F., & Zarzycki, C. M. (2022). Attribution of 2020 hurricane season extreme rainfall to human-induced climate change. *Nature Communications*, 13(1), 1905. <https://doi.org/10.1038/s41467-022-29379-1>
- Reyes, A. R., & Yang, D. (2021). Spontaneous cyclogenesis without radiative and surface-flux feedbacks. *Journal of the Atmospheric Sciences*, 78.
- Rios, G., Vecchi, G., & Yang, W. (2025a). Datasets used in analysis for publication “reducing tropical cyclone activity in global climate models by evaporative suppression”. <https://doi.org/10.5281/zenodo.14623457>
- Rios, G., Vecchi, G., & Yang, W. (2025b). GFDL GCM source code modifications for the Swishe algorithm. *Zenodo*. <https://doi.org/10.5281/zenodo.15832217>
- Rotunno, R., & Emanuel, K. A. (1987). An air-sea interaction theory for tropical cyclones. Part II: Evolutionary study using a nonhydrostatic axisymmetric numerical model. *Journal of the Atmospheric Sciences*, 44(3), 542–561. [https://doi.org/10.1175/1520-0469\(1987\)044<542:AAITFT>2.0.CO;2](https://doi.org/10.1175/1520-0469(1987)044<542:AAITFT>2.0.CO;2)
- Sanford, T. B., Black, P. G., Haustein, J. R., Feeney, J. W., Forristall, G. Z., & Price, J. F. (1987). Ocean response to a hurricane. Part I: Observations. *Journal of Physical Oceanography*, 17(11), 2065–2083. [https://doi.org/10.1175/1520-0485\(1987\)017<2065:ORTAHP>2.0.CO;2](https://doi.org/10.1175/1520-0485(1987)017<2065:ORTAHP>2.0.CO;2)
- Schenkel, B. A., & Hart, R. E. (2015). An examination of the thermodynamic impacts of western North Pacific tropical cyclones on their tropical tropospheric environment. *Journal of Climate*, 28(19), 7529–7560. <https://doi.org/10.1175/JCLI-D-14-00780.1>
- Schreck, C. J. III, Knapp, K. R., & Kossin, J. P. (2014). The impact of best track discrepancies on global tropical cyclone climatologies using ibtracs. *Monthly Weather Review*, 142(10), 3881–3899. <https://doi.org/10.1175/mwr-d-14-00021.1>
- Scoccimarro, E., Gualdi, S., Bellucci, A., Peano, D., Cherchi, A., Vecchi, G. A., & Navarra, A. (2020). The typhoon-induced drying of the Maritime Continent. *Proceedings of the National Academy of Sciences*, 117(8), 3983–3988. <https://doi.org/10.1073/pnas.1915364117>
- Scoccimarro, E., Gualdi, S., Bellucci, A., Sanna, A., Giuseppe Fogli, P., Manzini, E., et al. (2011). Effects of tropical cyclones on ocean heat transport in a high-resolution coupled general circulation model. *Journal of Climate*, 24(16), 4368–4384. <https://doi.org/10.1175/2011JCLI4104.1>
- Scoccimarro, E., Gualdi, S., Villarini, G., Vecchi, G. A., Zhao, M., Walsh, K., & Navarra, A. (2014). Intense precipitation events associated with landfalling tropical cyclones in response to a warmer climate and increased CO₂. *Journal of Climate*, 27(12), 4642–4654. <https://doi.org/10.1175/jcli-d-14-00065.1>
- Shen, L.-Z., Wu, C.-C., & Judt, F. (2021). The role of surface heat fluxes on the size of Typhoon Megi (2016). *Journal of the Atmospheric Sciences*, 78(4), 1075–1093. <https://doi.org/10.1175/JAS-D-20-0141.1>
- Sobel, A. H., & Camargo, S. J. (2005). Influence of western North Pacific tropical cyclones on their large-scale environment. *Journal of the Atmospheric Sciences*, 62(9), 3396–3407. <https://doi.org/10.1175/JAS3539.1>
- Sriver, R. L., & Huber, M. (2007). Observational evidence for an ocean heat pump induced by tropical cyclones. *Nature*, 447(7144), 577–580. <https://doi.org/10.1038/nature05785>
- Sriver, R. L., & Huber, M. (2010). Modeled sensitivity of upper thermocline properties to tropical cyclone winds and possible feedbacks on the Hadley circulation. *Geophysical Research Letters*, 37(8), 2010GL042836. <https://doi.org/10.1029/2010GL042836>
- Stramma, L., Cornillon, P., & Price, J. F. (1986). Satellite observations of sea surface cooling by hurricanes. *Journal of Geophysical Research*, 91(C4), 5031–5035. <https://doi.org/10.1029/JC091iC04p05031>
- Sun, J., Vecchi, G., & Soden, B. (2021). Sea surface salinity response to tropical cyclones based on satellite observations. *Remote Sensing*, 13(3), 420. <https://doi.org/10.3390/rs13030420>
- Tang, B., & Emanuel, K. (2010). Midlevel ventilation’s constraint on tropical cyclone intensity. *Journal of the Atmospheric Sciences*, 67(6), 1817–1830. <https://doi.org/10.1175/2010jas3318.1>
- Taylor, K. E., Stouffer, R. J., & Meehl, G. A. (2012). An overview of CMIP5 and the experiment design. *Bulletin of the American Meteorological Society*, 93(4), 485–498. <https://doi.org/10.1175/bams-d-11-00094.1>
- Vecchi, G. A., Delworth, T., Gudgel, R., Kapnick, S., Rosati, A., Wittenberg, A. T., et al. (2014). On the seasonal forecasting of regional tropical cyclone activity. *Journal of Climate*, 27(21), 7994–8016. <https://doi.org/10.1175/JCLI-D-14-00158.1>
- Walsh, K. J., McBride, J. L., Klotzbach, P. J., Balachandran, S., Camargo, S. J., Holland, G., et al. (2016). Tropical cyclones and climate change. *Wiley Interdisciplinary Reviews: Climate Change*, 7(1), 65–89. <https://doi.org/10.1002/wcc.371>
- Wang, D., & Lin, Y. (2020). Size and structure of dry and moist reversible tropical cyclones. *Journal of the Atmospheric Sciences*, 77(6), 2091–2114. <https://doi.org/10.1175/JAS-D-19-0229.1>
- Wing, A. A., Camargo, S. J., Sobel, A. H., Kim, D., Moon, Y., Murakami, H., et al. (2019). Moist static energy budget analysis of tropical cyclone intensification in high-resolution climate models. *Journal of Climate*, 32(18), 6071–6095. <https://doi.org/10.1175/JCLI-D-18-0599.1>
- Yano, J.-I., & Emanuel, K. (1991). An improved model of the equatorial troposphere and its coupling with the stratosphere. *Journal of the Atmospheric Sciences*, 48(3), 377–389. [https://doi.org/10.1175/1520-0469\(1991\)048<377:AIMOTE>2.0.CO;2](https://doi.org/10.1175/1520-0469(1991)048<377:AIMOTE>2.0.CO;2)
- Zhang, B., Soden, B. J., Vecchi, G. A., & Yang, W. (2021). The role of radiative interactions in tropical cyclone development under realistic boundary conditions. *Journal of Climate*, 34(6), 2079–2091. <https://doi.org/10.1175/JCLI-D-20-0574.1>
- Zhang, F., & Emanuel, K. (2016). On the role of surface fluxes and WISHE in tropical cyclone intensification. *Journal of the Atmospheric Sciences*, 73(5), 2011–2019. <https://doi.org/10.1175/JAS-D-16-0011.1>
- Zhang, W., Vecchi, G. A., Murakami, H., Delworth, T., Wittenberg, A. T., Rosati, A., et al. (2016). Improved simulation of tropical cyclone responses to ENSO in the western north pacific in the high-resolution GFDL HIFLOR coupled climate model. *Journal of Climate*, 29(4), 1391–1415. <https://doi.org/10.1175/jcli-d-15-0475.1>
- Zhao, M., Held, I. M., & Lin, S.-J. (2012). Some counterintuitive dependencies of tropical cyclone frequency on parameters in a GCM. *Journal of the Atmospheric Sciences*, 69(7), 2272–2283. <https://doi.org/10.1175/JAS-D-11-0238.1>
- Zhao, M., Held, I. M., Lin, S.-J., & Vecchi, G. A. (2009). Simulations of global hurricane climatology, interannual variability, and response to global warming using a 50-km resolution GCM. *Journal of Climate*, 22(24), 6653–6678. <https://doi.org/10.1175/2009JCLI3049.1>